MITSUBISHI ELECTRIC RESEARCH LABORATORIES
https://www.merl.com

A Sparsity-Driven Method to Iteratively Extract Motor Fault Signatures in Varying-Speed Operations

Liu, Dehong; Wang, Yebin; Shinya, Tsurutashin

TR2024-162 November 28, 2024

Abstract

Motors are typically operating at varying speed conditions, especially when they are driven by inverters for high efficiency. However, it is challenging to detect motor faults under varying operating conditions due to the frequency variation of fault signatures, spectrum distortion, and other interference. Even the fault signature is extracted, the fault severity is often underestimated and not robust. To address these issues, we propose a sparsity-driven method to iteratively extract speed- dependent fault frequency components from the stator current, considering frequency variation due to varying speed. Experiments show that our method can extract frequency signatures of different faults with significantly better results compared to other state-of-the-art methods. The proposed method can be applied to inverter-fed motor drive system for robust fault detection.

International Conference on Electrical Machines and Systems (ICEMS) 2024

Mitsubishi Electric Research Laboratories, Inc.
201 Broadway, Cambridge, Massachusetts 02139

A Sparsity-Driven Method to Iteratively Extract Motor Fault Signatures in Varying-Speed Operations

Dehong Liu, Yebin Wang, and Shinya Tsuruta
Mitsubishi Electric Research Laboratories, Cambridge, MA, USA

***Abstract*—Motors are typically operating at varying speed conditions, especially when they are driven by inverters for high efficiency. However, it is challenging to detect motor faults under varying operating conditions due to the frequency variation of fault signatures, spectrum distortion, and other interference. Even the fault signature is extracted, the fault severity is often underestimated and not robust. To address these issues, we propose a sparsity-driven method to iteratively extract speed-dependent fault frequency components from the stator current, considering frequency variation due to varying speed. Experiments show that our method can extract frequency signatures of different faults with significantly better results compared to other state-of-the-art methods. The proposed method can be applied to inverter-fed motor drive system for robust fault detection.**

***Index Terms*—Motor fault, Fault signature, Varying speed operation, Sparse signal**

I. Introduction

Induction motors are important drive machines for industries because they are cost-effective, endurable for various environmental conditions, and relatively efficient. However, after long-time (like years) of operations, induction motors may develop mechanical and electrical faults, such as bearing fault, broken bar fault, eccentricity, insulation deterioration, and short circuit, *etc*. These faults degrade the performance of motors in general. For example, mechanical faults may cause vibration, torque ripple, and sound noise, resulting a lower efficiency. If the faulty motor is not well maintained or repaired in time, it may even lead to sudden catastrophic failure. Therefore, it is important to detect faults, estimate their severity, and perform timely maintenance to minimize potential loss.

To detect motor faults, the most popular way is to extract fault signatures by analyzing the stator current frequency spectrum, or so-called motor current signature analysis (MCSA) [1]. In healthy conditions, the stator current of a three-phase induction motor includes the operating frequency component, which is typically 50Hz (or 60Hz), and its higher-order harmonics. The operating frequency current generates a symmetric and rotating magnetic field in the air gap between the stator and the rotor. When a motor fault occurs, the magnetic field generated by the three-phase stator current is not symmetric any more. Consequently, extra frequency components are induced in the stator current, with different faults corresponding to different frequency components. Therefore, motor faults can be detected by extracting the corresponding fault signature in the frequency domain. Furthermore, the fault severity is estimated according to the ratio between the fault frequency magnitude and the operating frequency magnitude. A larger ratio indicates a bigger asymmetry of magnetic field, and therefore a more severe fault. Since the MCSA-based method does not need other sensor data but the stator current for detection, it is non-invasive and cost-effective for health monitoring.

However, motors are typically operating at varying-speed conditions, which fact makes fault detection a challenging problem [2]–[4]. First, fault signatures in the frequency domain are typically speed-dependent. Varying-speed operation means varying fault frequency. Second, the factor between the fault frequency and the speed is fault-dependent. Under the same speed variation, different fault signatures may have different frequency variation ranges. Therefore, it is also not suitable to extract fault frequency within a fixed frequency range. Third, under varying-speed operations, the fault frequency component energy is spread out in a frequency range, depending on the speed profile pattern. The spread fault frequency energy lowers down the ratio between the magnitude of fault frequency and the magnitude of operating frequency. Consequently, a fault may not be detected according to a preset threshold suitable for steady operation conditions. Even if the fault is detected, its severity level may be underestimated.

It is an essential problem to extract proper fault signatures that is robust to speed variations for further analysis. To deal with the fault signature extraction problem, a blind deconvolution demodulation method [5] is proposed to deblur the fault signature for motors operating at varying speed and varying load conditions. However, it is only valid for one specific fault type where the corresponding fault frequency components have the same variation pattern, but not for a mix of multiple fault types. Other methods such as graph based method [6] considers the smoothness and sparsity of the fault signature, purely from signal processing, not from the physical model point of view. In recent years, artificial intelligence (AI) and machine learning has been extensively applied in many areas including motor fault detection and diagnosis, where physical model-based features, such as motor current signature, play an important role [2], [7], [8]. Fault features that are robust to operating conditions are preferred to facilitate the complexity of machine learning algorithms and improve the overall performance.

In this paper, a robust method is proposed to analyze stator current of motor operating at varying speed conditions with

a mix of multiple faults. The main contributions of this paper are summarized as follows.

- A physical model-based, sparsity-driven method is proposed to iteratively extract the operating frequency component and its harmonics, speed-dependent slot harmonics related to eccentricity fault and bearing fault, and speed-dependent broken-bar fault frequency components from noisy stator current.
- Analysis on speed-dependent fault signatures is performed to achieve a speed-independent and load-independent fault feature such that different faults can be detected and their severity can be properly estimated.
- With the proposed sparsity-driven method, small fault signatures are extracted from noisy measurements. This is helpful to detect early-stage faults for predictive maintenance.

II. Motor current signature

A. Constant-speed operation

We consider an inverter-fed motor operating at a constant speed with a fixed load. In general, the motor current includes the fundamental operating frequency component and its harmonics at healthy condition. The time-domain stator current can be formulated as

$$i_h(t) = I_{s,1}\cos(2\pi f_s t + \phi_s) + \sum_n I_{s,n}\cos(2\pi f_{s,n} t + \phi_{s,n}), \tag{1}$$

where f_s is the operating frequency, $I_{s,1}$ is the current amplitude of operating frequency, ϕ_s is the initial phase of the operating frequency component, and subscript n represents the order of harmonics.

When a motor fault occurs, additional fault frequency components will be induced in the stator current

$$i_f(t) = i_h(t) + \sum_l I_{f,l}\cos(2\pi f_{f,l} t + \phi_{f,l}), \tag{2}$$

where $I_{f,l}$ represents the amplitude of the lth fault frequency component $f_{f,l}$, and $\phi_{f,l}$ is the initial phase of the lth fault frequency component.

Extensive research work has been done in identifying the fault frequency based on different physical models. For example, when there exists a broken-bar fault in a squirrel-cage induction motor, the fault frequency can be expressed as [9]

$$f_{bar} = (1 \pm 2\tau s) f_s, \tag{3}$$

where $\tau = 1, 2, \ldots$, and s is the motor slip, which can be calculated using the motor n_r and the synchronous speed n_s as $s = 1 - \frac{n_r}{n_s}$.

For bearing fault, depending on the fault location in the bearing and the bearing size, the characteristic fault frequency induced in the stator current is proportional to the mechanical frequency of the rotor $f_r = \frac{1-s}{p} f_s$, *i.e.* [10]

$$f_b \propto \frac{1-s}{p} f_s. \tag{4}$$

For eccentricity fault in most induction machines, it can be identified using slot harmonics in the current [11], [12]

$$f_{slt} = ((\kappa Z \pm n_d)\frac{1-s}{p} + \nu) f_s, \tag{5}$$

where Z is the number of rotor slots; p is number of pole pairs; $\kappa = 1, 2, 3, ...$; n_d is the eccentricity order ($n_d = 0$ in case of static eccentricity and $n_d = 1, 2, 3, ...$, in case of dynamic eccentricity); and $\nu = \pm 1, \pm 3, \pm 5, ...$ is the order of stator time harmonics.

When the motor is operating at a constant speed and a constant load, all these fault frequencies are of fixed values. Therefore, for most motor fault detection problems, the objective of MCSA-based methods is to extract the corresponding fault signature components via effectively frequency spectral analysis. Once a fault frequency component over a certain threshold is detected, its corresponding fault is claimed. The fault severity can be further estimated according to the ratio between the magnitude of the fault frequency component and that of the operating frequency component.

Let $i_s(t)$ represent the time-domain stator current of a motor in an ideal steady-state operation. Note that the current could be a single-phase current or a combination of three phase current after proper phase alignment such as Park transform.

The frequency spectrum of the stator current i_s (i_h for healthy condition or i_f for faulty condition) can be achieved by the Fourier transform as

$$I_s(\omega) = \int i_s(t) e^{-j\omega t} dt. \tag{6}$$

For periodic signals, a discrete Fourier transform (DFT) is typically used to compute the Fourier spectrum based on discrete time samplings $i_s(n)$. We ignore the detailed correspondence between the frequency and the sampling rate, and simplify the expression of Fourier spectrum as

$$[I(n_f)] = DFT[i_s(n_t)], \tag{7}$$

where n_t and n_f represent discrete time and frequency respectively.

B. Varying-speed operations

From Sec.II-A we observe that all aforementioned motor fault signatures are related to the motor slip s. When the motor is operating at varying-speed conditions, the fault frequency changes accordingly.

To demonstrate the impact of varying speed to motor fault detection, we show two examples of stator current spectra of a faulty motor operating at a varying speed in Fig.1. When 2.5 second length current is collected, its Fourier spectrum is shown in Fig. 1 (a). The spectrum magnitude is normalized by the operating frequency magnitude. We observe a frequency component around 46Hz with a normalized magnitude of -39.3dB. With normalized noise spectrum floor around -45dB, it is uncertain whether this 46Hz component is a broken-bar fault signature or just noise. When we collect longer-time current of about 50 seconds, the corresponding Fourier spectrum is shown in Fig. 1 (b). It is clear that the

noise spectrum floor reduces to -60dB due to longer-time measurements. However, the maximum sideband component also reduces to a lower level, at frequency 42.7Hz with magnitude of -49.2dB, almost 10dB lower than that shown in Fig. 1 (a) of a short-time window. Clearly, if a preset threshold is used for this fault detection, different detection results or different severity levels will be claimed for the same motor but with different lengths of measurements.

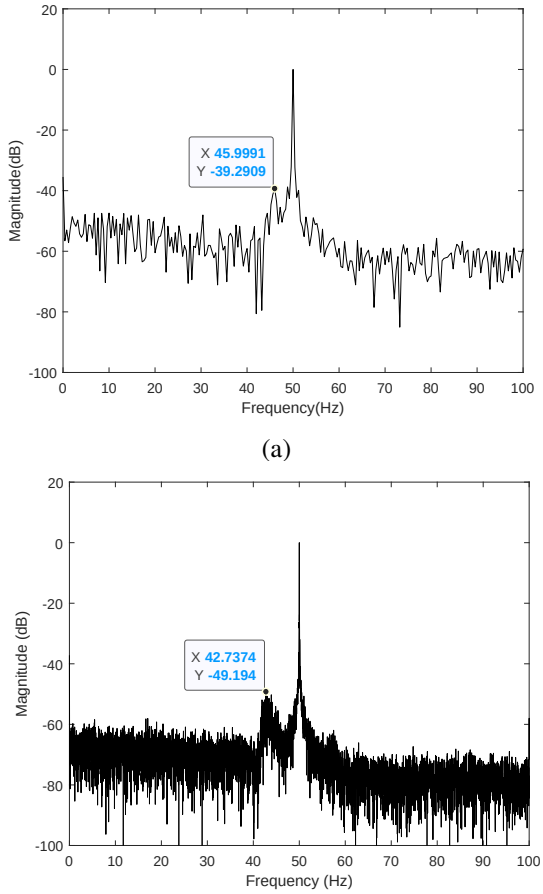

Fig. 1. Frequency spectra of stator current in varying operating condition using Fourier transform with (a) 2.5 second time window measurement and (b) 50 second time window measurement.

Further investigation shows that due to the varying speed operation, the fault frequency changes in a small range accordingly. According to Parseval's theorem, the sum (or integral) of the square of a time-domain signal is equal to the sum (or integral) of the square of its Fourier transform. Therefore, as more measurements are collected in the time-domain, the operating frequency energy accumulates at a fixed operating frequency point in the Fourier domain, while the fault frequency energy is distributed in a frequency range depending on the speed change. Ultimately, the ratio between the fault frequency component and the operating frequency component decreases to a lower level depending on the motor speed range. Similar phenomena happen to other faults.

Although the Fourier spectrum of a short-time window may provide the right ratio, the spectrum is very noisy, and may be influenced by other interference. In practice, an empirical threshold is set to detect the fault, but the fault severity may be underestimated. Therefore, a proper way to deal with this issue is to adaptively align the fault frequency of short-time windows such that the overall fault frequency energy can be added up. Following this idea, we proposed a physical-model based, sparsity-driven method to iteratively extract fault signatures.

III. Proposed Method

To capture the frequency variation of fault signatures, short-time Fourier transform (STFT) is used for spectral analysis, with N overlapped sliding time windows on the time-domain current. Assume that the motor speed can be treated as a constant in a short-time window used for spectral analysis. Given the STFT spectrum, we further exploit frequency variations of different time windows using advanced sparsity-driven signal processing techniques. The detail of our proposed method is described in the following section.

For fault frequency detection at varying speed conditions, an essential task is to align the fault frequency component in the frequency domain such that those formula for constant speed operations can be used to extract the fault frequency component. Note that fault signature magnitudes are typically much smaller than that of the operating frequency signal. Besides that, measurement noise and interference from other equipment such as inverters also makes the fault frequency alignment more challenging. To improve the robustness, we exploit the relationship of frequency variations of different time windows and iteratively extract signals according to their physical property such that fault signals can be well estimated.

A. Frequency variation Estimation

For those fault signals of varying frequency due to speed variation, we propose the following robust method to estimate the frequency variation such that the fault frequency of different time windows can be well aligned.

For example, according to (5), slot harmonic frequency variation due to speed variation can be represented as

$$\Delta f_{slt} = (\kappa Z \pm n_d)\frac{f_s}{pn_s}\Delta n_r = \frac{\kappa Z \pm n_d}{60}\Delta n_r. \qquad (8)$$

Note that the frequency variation in (8) is independent of the order of stator time harmonics, meaning that all orders of slot harmonics will have the same frequency variation given a speed change. Without loss of generality, let $\mathbf{h}_k = [\Delta f_{k,1}, ..., \Delta f_{k,i}, ..., \Delta f_{k,N}]^\top$ be a column vector of the kth fault frequency variation across all time windows, in which the ith entry $\mathbf{h}_k(i) = \Delta f_{k,i}$ is the frequency variation of kth fault frequency in the ith time window. It is clear that $\mathbf{h}_k = \mathbf{0}$ for steady constant-speed operations. The fault frequency difference between the ith and the jth time windows due to speed variation is

$$L_k(i,j) = \mathbf{h}_k(i) - \mathbf{h}_k(j), \quad \text{for} \quad i,j = 1,2,\cdots,N;\ k = 1,2,\cdots,K. \qquad (9)$$

In many applications such as speed sensorless drive, the speed is not directly measured and needs to be estimated.

Here we aim to extract the fault frequency without any information about the varying speed.

Let $[I_i(n_f)]$ be the frequency spectrum of the ith ($i = 1, ..., N$) time window stator current and $[I_{k,i}(n_f)]$ be a cropped spectrum covering the kth fault signature frequency variation range based on its physical model. In theory, it is straightforward to find the frequency difference by computing the cross correlation between the frequency spectrum of the ith time window signal $[I_{k,i}(n_f)]$ and that of the jth time window signal $[I_{k,j}(n_f)]$ as

$$\hat{L}_k(i,j) = \text{argmax}_{n_d} \sum_{n_f} |I_{k,i}(n_f)| \cdot |I_{k,j}(n_f + n_d)|. \quad (10)$$

In practice, since the fault signal is very weak and sensitive to noise interference, the solution of (10) may be not accurate or even far away from the true value. Here we use $\hat{L}_k$ to represent the estimated frequency variation from noisy measurements according to (10), and L_k to represent the underlying true frequency variation. Our objective is then to recover $\mathbf{h}_k$ from a set of all estimations $\{\hat{L}_k\}$.

To improve the robustness, we further define a matrix $\mathbf{L}_k = [L_k(i,j)] \in \mathbb{R}^{N \times N}$ and its concatenated vector $l_k = [L_k(1,1), ..., L_k(i,j), ..., L_k(N,N)]^\top \in \mathbb{R}^{N^2 \times 1}$. We rewrite the matrix as

$$\mathbf{L}_k = \mathbf{h}_k \mathbf{1}^\top - \mathbf{1}\mathbf{h}_k^\top \in \mathbb{R}^{N \times N}, \quad (11)$$

where $\mathbf{1}$ is an N-dimensional vector with all entries equal to 1. For any real vector $\mathbf{h}_k$, we have

$$\text{rank}(\mathbf{L}_k) \leq \text{rank}(\mathbf{h}_k \mathbf{1}^\top) + \text{rank}(\mathbf{1}\mathbf{h}_k^\top) = 2. \quad (12)$$

From (12) we conclude that in theory the matrix of frequency variation is a low-rank (rank≤ 2) matrix. However, in practice the estimated matrix $\hat{\mathbf{L}}$ using (10) is not low-rank due to estimation errors. An effective way to recover $\mathbf{h}$ from noisy $\hat{\mathbf{L}}$ is to use the well-known robust PCA method [13], which decomposes the observation matrix $\hat{\mathbf{L}}$ into a low-rank matrix and a sparse noise matrix. However, it is not guaranteed that the low-rank matrix decomposed by the robust PCA method is in the form of (11). Here instead of using the robust PCA, we implicitly impose low rankness.

We can express l_k as

$$l_k = \mathbf{A}\mathbf{h}_k, \quad (13)$$

with

$$\mathbf{A} = [\cdots, \alpha_{i,j}, \cdots]^\top \in \mathbb{R}^{N^2 \times N}, \quad (14)$$

where vector $\alpha_{i,j} \in \mathbb{R}^{1 \times N}$ has all-zero entries except that $\alpha_{i,j}(i) = 1$ and $\alpha_{i,j}(j) = -1$. Consequently, the frequency variation estimation problem is formulated as

$$\min_{\mathbf{e}, \mathbf{h}_k} \frac{1}{2} \|\hat{l}_k - \mathbf{A}\mathbf{h}_k - \mathbf{e}\|_2^2 + \lambda |\mathbf{e}|_1, \quad (15)$$

where λ is the regularization parameter and vector $\mathbf{e}$ represents large frequency variation error cause by interference. It is clear that when $\lambda = 0$ and $\mathbf{e} = \mathbf{0}$, (15) is reduced to the least-squares method. When the interference is Gaussian noise, the least-squares method works well. In our case, where there exists other interference introduced by the inverter, sparsity-inspired optimization in (15) improves the robustness.

To solve (15), we utilize the alternating minimization method by iteratively updating $\mathbf{e}$ and $\mathbf{h}_k$ until its stopping criteria is satisfied. The sub-problem with respect to $\mathbf{h}_k$ is a standard least-squares problem, which can be solved by

$$\mathbf{h}_k^{(t)} = \mathbf{A}^+ (\hat{l}_k - \mathbf{e}^{(t-1)}), \quad (16)$$

where $\mathbf{A}^+$ denotes the pseudo-inverse of $\mathbf{A}$, and superscripts (t) and $(t-1)$ represent the number of iterations during the process.

The sub-problem of $\mathbf{e}$ can be solved by a soft-thresholding process as [14]

$$\mathbf{e}^{(t)} = \max(0, |\hat{l}_k - \mathbf{A}\mathbf{h}_k^{(t)}| - \lambda) \odot \text{sign}(\hat{l}_k - \mathbf{A}\mathbf{h}_k^{(t)}). \quad (17)$$

Once the kth fault frequency variation vector $\hat{\mathbf{h}}_k = \mathbf{h}_k^{(T)}$ is properly estimated, we can align the spectrum by shifting the frequency spectrum of the ith time window by $-\hat{\mathbf{h}}_k(i)$ circularly, *i.e.*,

$$[\bar{I}_{k,i}(n_f)] = \text{circshift}([I_i(n_f)], -\hat{\mathbf{h}}_k(i)), \quad (18)$$

and form a matrix of aligned spectra as

$$\bar{\mathbf{I}}_k = [[\bar{I}_{k,1}(n_f)], ..., [\bar{I}_{k,i}(n_f)], ..., [\bar{I}_{k,N}(n_f)]], \quad (19)$$

where the kth fault frequency is aligned.

B. Frequency component Extraction

After compensating the frequency variation of the kth fault signature, the kth fault signature apprears in a row of the spectrogram matrix $\bar{\mathbf{I}}_k$. Therefore, the kth fault frequency should be included in the left principal singular vector of $\bar{\mathbf{I}}_k$. Following this idea, we perform singular value decomposition (SVD) on $\bar{\mathbf{I}}_k$

$$\bar{\mathbf{I}}_k = \mathbf{U}_k \mathbf{\Sigma}_k \mathbf{V}_k^\top = \sum_j \sigma_{k,j} \mathbf{u}_{k,j} \mathbf{v}_{k,j}^\top. \quad (20)$$

The kth speed-independent frequency component of stator current is then achieved by simply thresholding the magnitude of $\mathbf{u}_{k,1}$ to keep the largest frequency component, *i.e.*,

$$\hat{\mathbf{u}}_{k,1} = \text{threshold}(\mathbf{u}_{k,1}). \quad (21)$$

Note that $\hat{\mathbf{u}}_{k,1}$ is independent to the operating speed due to the fault frequency alignment, and therefore it equivalent to the spectrum at constant-speed operation. The fault signature extraction process does not require information of the speed and suitable for any varying speed patterns. Therefore it is robust for varying speed operations.

For comparison, the denoised kth speed-dependent frequency component is achieved by shifting $\hat{\mathbf{u}}_{k,1}$ to its original speed-dependent frequency as

$$[\hat{I}_{k,i}(n_f)] = \text{circshift}\{[\sigma_{k,1} \hat{\mathbf{u}}_{k,1} \mathbf{v}_{k,1}^\top(i)], \hat{\mathbf{h}}_k(i)\}. \quad (22)$$

C. Iterative frequency component extraction

Based on the frequency variation estimation method in Sec. III-A, we iteratively align frequency components in frequency spectra of short-time windows and extract them as equivalent frequency components of steady operations.

Considering the fundamental operating frequency is typically the strongest frequency component, we first extract the fundamental frequency and its harmonics. For fixed operating frequency, the fundamental frequency and its harmonics can be detected by examining the average magnitude. If the average magnitude is greater than a preset threshold with small variance, we treat the corresponding frequency as the operating frequency harmonics. For varying frequency operations, the fundamental frequency and its harmonics can be aligned by the method illustrated in Sec. III-A.

For slot harmonics which are related to eccentricity and other faults, we employ the proposed frequency variation estimation method to align slot harmonics and extract them from the aligned frequency spectra. Recalling that all slot harmonics are evenly separated by f_s according to (5), we can align and extract all slot harmonics simultaneously. Given the dominant slot harmonic of static eccentricity $n_d = 0$, motor speed can also be estimated as [15]

$$n_r = \frac{60}{Z}(f_{slt} - \nu f_s). \tag{23}$$

Similarly, for other speed-dependent fault signatures, we can align the fault frequency using the proposed sparsity-driven method and extract the frequency component using SVD decomposition. Since they are all related to the speed, an alternative way to the proposed method is to make use of the estimated frequency variation vector for slot harmonics. For example, it is straightforward to infer the broken-bar fault frequency variation in terms of slot harmonic frequency variation according to (3) and (5), *i.e.*,

$$\mathbf{h}_{k_b} = \pm\frac{2p}{Z}\mathbf{h}_{k_s}, \tag{24}$$

where the subscript integers k_s and k_b represent the serial numbers of slot harmonics and broken-bar fault frequency respectively. Given $\mathbf{h}_{k_b}$, two characteristic broken-bar fault frequency components indicated by (3) with $\tau = 1$ can be aligned and extracted respectively.

Once we have extracted all frequency components of interests, for comparison we can achieve the denoised STFT spectrum by adding all denoised *speed-dependent* frequency components in (22) as

$$[\hat{I}_i(n_f)] = [\sum_k [\hat{I}_{k,i}(n_f)]]. \tag{25}$$

The final equivalent Fourier spectrum of the whole time-domain measurement can be synthesized by combining all extracted *speed-independent* frequency components as

$$\hat{\mathbf{I}}_s = \sum_k \sigma_{k,1}\hat{\mathbf{u}}_{k,1}. \tag{26}$$

Since this spectrum is speed-independent and with a fixed fault frequency component to operating frequency component ratio, it is robust for motor fault detection and severity estimation.

IV. Experiments

A. Setup

To validate our method, we perform experiments on a 1HP three-phase squirrel-cage induction motor. The experimental setup is shown in Fig. 2. The motor is driven by a three-phase inverter. A servo-motor, whose speed and torque can be controlled precisely, is mounted on the induction motor shaft and well aligned with the induction motor to work as a load for the experiment. During operations, we fix the fundamental operating frequency and manually adjust the load torque (servo-motor) with an arbitrary pattern such that the motor speed changes accordingly with time. The three-phase stator currents are measured using current sensors and recorded via a dSPACE® Scalexio Labbox platform for further analysis.

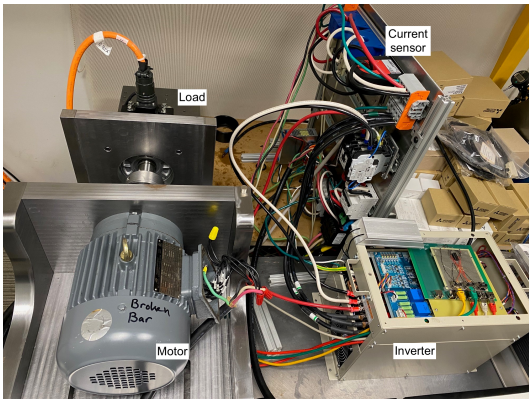

Fig. 2. Experimental setup.

B. Results

An example of the time-domain stator current of the motor operating at a varying-load and varying-speed condition is shown in Fig. 3, where we record about 53 second time-domain data with a sampling rate of 2kHz. It is clear that due to the varying load, the stator current amplitude also changes from time to time to meet the load requirement. We

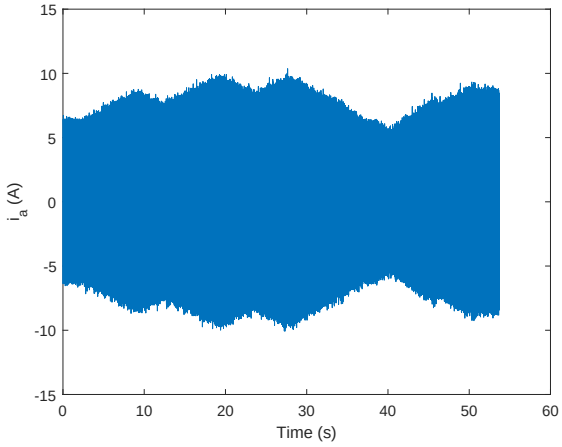

Fig. 3. Time-domain stator current.

perform STFT on stator current using a 2.5 second sliding time window, with 2 second overlap from window to window.

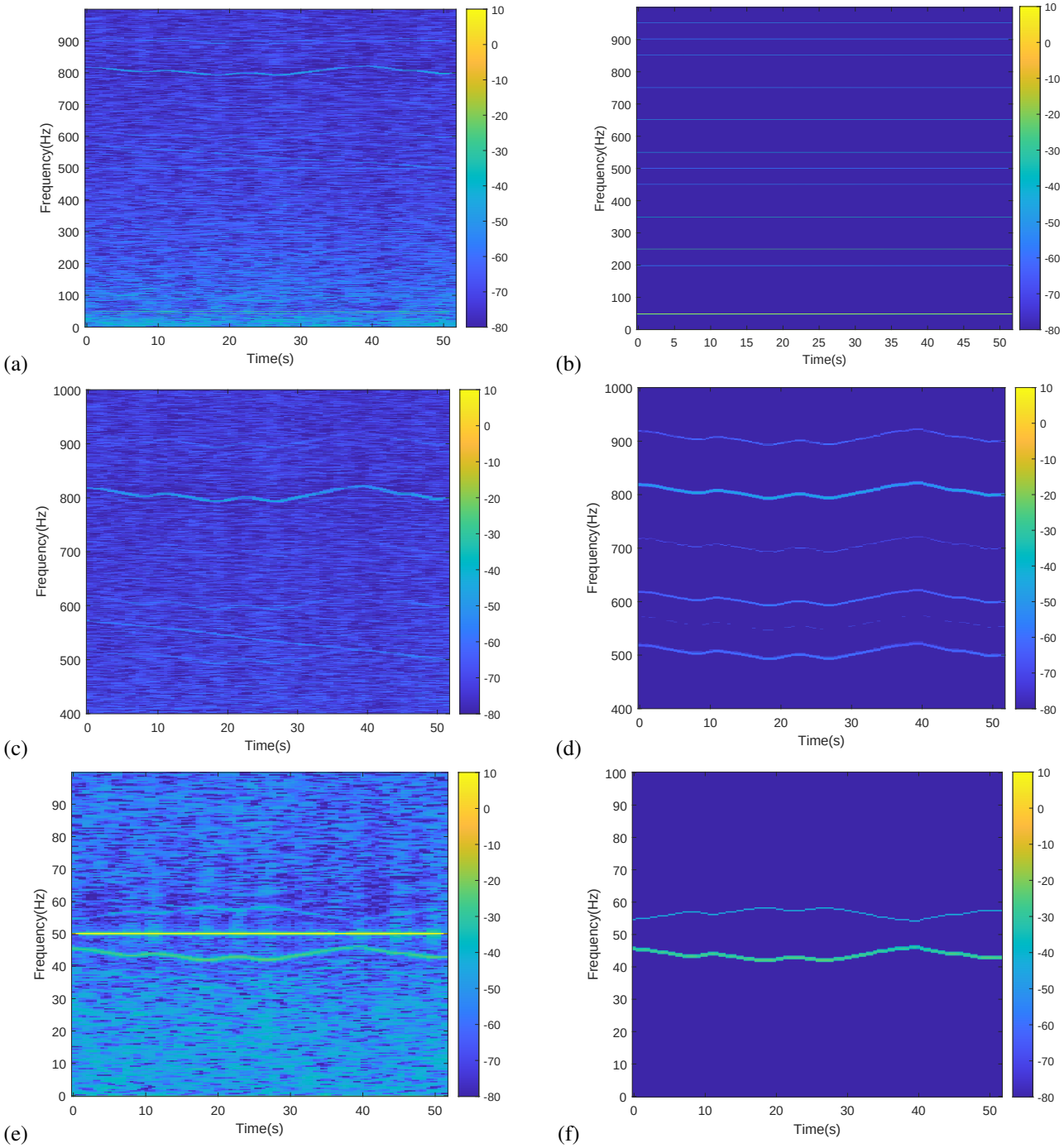

Fig. 4. Spectra of stator current in short-time windows. (a) Noisy spectrum in the frequency range of interest, (b) Extracted operating frequency component and its harmonics, (c)Noisy spectrum in the frequency range of slot harmonics, (d)Extracted slot harmonics, (e) Noisy spectrum in the frequency range of broken bar fault frequency, and (f) Extracted broken-bar fault frequency components.

The results are summarized in Fig. 4 with details described as follows. Fig. 4 (a) shows the STFT spectrum in the frequency range of interest. To improve detection performance, a minimum variance-based spectral analysis method [16] is considered in the post-process to suppress the noise and reduce the influence of varying load in the STFT spectrum. We then iteratively extract operating frequency and its harmonics, slot harmonics, and broken-bar fault frequencies. In Fig. 4 (b) we plot the extracted operating frequency and its harmonics. For comparison, in Fig. 4 (c) we plot a zoomed-in version of the STFT spectrum in the range of slot harmonics, and in Fig. 4 (d) we plot the extracted slot harmonics according to (22). We observe that all slot harmonics are very well extracted, even those very weak slot harmonics under strong interference indicated by the straight line in Fig. 4 (c) in the frequency range of $500 - 600$Hz. Similarly, in Fig. 4 (e) we plot a zoomed-in version of the STFT spectrum in the range of broken-bar fault frequencies, and plot the extracted

broken-bar fault frequencies in Fig. 4 (f), respectively. Again, both the characteristic fault frequency component and the secondary fault frequency component are extracted in the noisy measurement.

For MCSA-based fault detection, we typically consider the Fourier spectrum of stator current. Fig. 5 presents frequency spectra of the whole measurement of a large time window when the motor is operating at varying speed. For comparison, in Fig. 5 (a) we show the Fourier spectrum, where the operating frequency component magnitude is normalized, while in Fig. 5 (b) we show the equivalent spectrum using (26), where frequency components with different frequency variations are coded using different colors. We observe that the equivalent spectrum shows accurate fault signature magnitude, which agrees with that in the short-time Fourier spectrum shown in Fig. 5, but without noise interference. Due to varying speed operation, the broken-bar fault frequency magnitude and slot harmonic magnitude are all about 10dB lower than that of the equivalent spectrum at constant speed, which may cause mis-detection (false negative) in practice. Experimental results demonstrate that our proposed method can improve the performance of detection and severity estimation for motors operating at varying-speed and varying-load conditions.

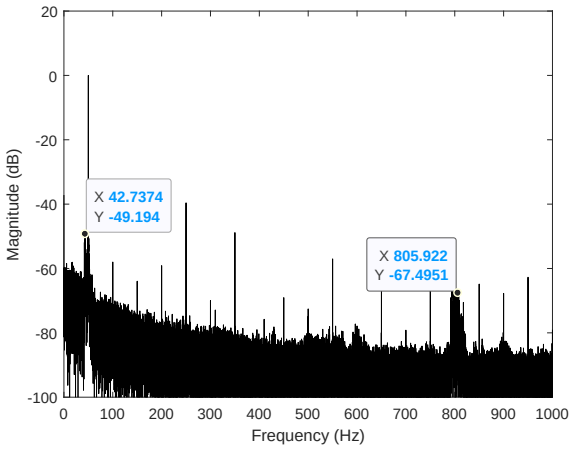

(a) Fourier spectrum at varying speed

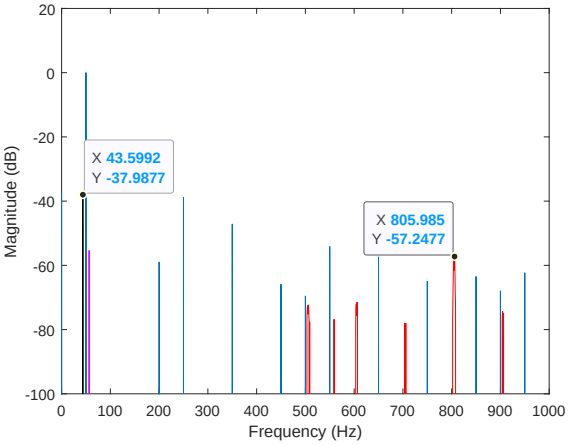

(b) Equivalent spectrum at a constant speed

Fig. 5. Frequency spectrum of stator current.

V. Conclusion

In this paper, we proposed a sparsity-driven method to iteratively extract frequency components from the stator current of a motor operating at varying speed conditions. We evaluated our method on experimental data for motor current signature analysis-based fault detection. Experimental results demonstrate that our method can effectively extract fault signatures of different types of faults under arbitrary unknown speed, with robust fault signature magnitude indicating the severity level. The denoising performance is significantly better than other existing methods.

References

[1] W. T. Thomson and M. Fenger, "Current signature analysis to detect induction motor faults," *IEEE Industry Applications Magazine*, vol. 7, no. 4, pp. 26–34, 2001.

[2] I. Martin-Diaz, D. Morinigo-Sotelo, O. Duque-Perez, and R. J. Romero-Troncoso, "An experimental comparative evaluation of machine learning techniques for motor fault diagnosis under various operating conditions," *IEEE Transactions on Industry Applications*, vol. 54, no. 3, pp. 2215–2224, 2018.

[3] M. Z. Ali, M. N. S. K. Shabbir, S. M. K. Zaman, and X. Liang, "Single-and multi-fault diagnosis using machine learning for variable frequency drive-fed induction motors," *IEEE Transactions on Industry Applications*, vol. 56, no. 3, pp. 2324–2337, 2020.

[4] A. Stefani, A. Bellini, and F. Filippetti, "Diagnosis of induction machines' rotor faults in time-varying conditions," *IEEE Transactions on Industrial Electronics*, vol. 56, no. 11, pp. 4548–4556, 2009.

[5] V. A. Kelkar, D. Liu, H. Inoue, and M. Kanemaru, "Sparsity-driven joint blind deconvolution-demodulation with application to motor fault detection," in *ICASSP 2023-2023 IEEE International Conference on Acoustics, Speech and Signal Processing (ICASSP)*. IEEE, 2023.

[6] D. Liu, V. Anantaram, and A. Goldsmith, "Extracting broken-rotor-bar fault signature of varying-speed induction motors," in *PHM Society Asia-Pacific Conference*, vol. 4, no. 1, 2023.

[7] J. E. Garcia-Bracamonte, J. M. Ramirez-Cortes, J. de Jesus Rangel-Magdaleno, P. Gomez-Gil, H. Peregrina-Barreto, and V. Alarcon-Aquino, "An approach on MCSA-based fault detection using independent component analysis and neural networks," *IEEE Transactions on Instrumentation and Measurement*, vol. 68, no. 5, pp. 1353–1361, 2019.

[8] X. Zheng, H. Inoue, M. Kanemaru, and D. Liu, "Eccentricity severity estimation of induction machines using a sparsity-driven regression model," in *2022 IEEE Energy Conversion Congress and Exposition (ECCE)*, 2022, pp. 1–6.

[9] F. Filippetti, G. Franceschini, C. Tassoni, and P. Vas, "AI techniques in induction machines diagnosis including the speed ripple effect," *IEEE Transactions on Industry Applications*, vol. 34, no. 1, pp. 98–108, 1998.

[10] S. Zhang, B. Wang, M. Kanemaru, C. Lin, D. Liu, M. Miyoshi, K. H. Teo, and T. G. Habetler, "Model-based analysis and quantification of bearing faults in induction machines," *IEEE Transactions on Industry Applications*, vol. 56, no. 3, pp. 2158–2170, 2020.

[11] P. Vas, *Parameter estimation, condition monitoring, and diagnosis of electrical machines*. Oxford University Press, 1993, vol. 27.

[12] K. D. Hurst and T. G. Habetler, "Sensorless speed measurement using current harmonic spectral estimation in induction machine drives," *IEEE Transactions on Power Electronics*, vol. 11, no. 1, pp. 66–73, 1996.

[13] E. J. Candès, X. Li, Y. Ma, and J. Wright, "Robust principal component analysis?" *Journal of the ACM (JACM)*, vol. 58, no. 3, pp. 1–37, 2011.

[14] D. L. Donoho, "De-noising by soft-thresholding," *IEEE transactions on information theory*, vol. 41, no. 3, pp. 613–627, 1995.

[15] W. L. Silva, A. M. N. Lima, and A. Oliveira, "Speed estimation of an induction motor operating in the nonstationary mode by using rotor slot harmonics," *IEEE Transactions on Instrumentation and Measurement*, vol. 64, no. 4, pp. 984–994, 2014.

[16] D. Liu, H. Inoue, and M. Kanemaru, "Robust motor current signature analysis (MCSA)-based fault detection under varying operating conditions," in *2022 25th International Conference on Electrical Machines and Systems (ICEMS)*. IEEE, 2022, pp. 1–5.